PAPER

Atomic layer deposition of Al-doped ZnO nanomembrane with *in situ* monitoring

To cite this article: Jinlong Wang *et al* 2024 *Nanotechnology* **35** 405704

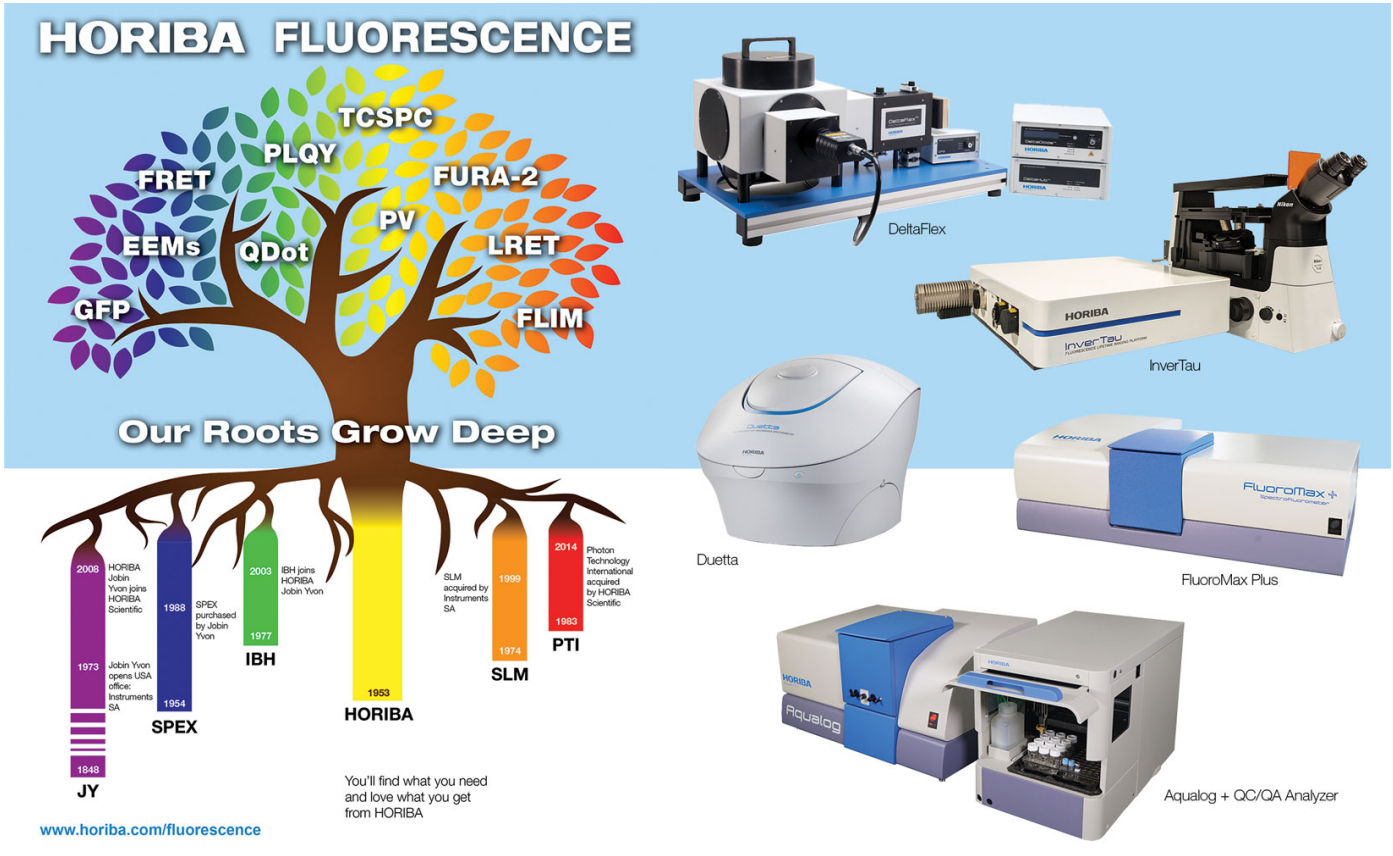

IOP Publishing Nanotechnology

Nanotechnology **35** (2024) 405704 (9pp) https://doi.org/10.1088/1361-6528/ad60ce

Atomic layer deposition of Al-doped ZnO nanomembrane with *in situ* monitoring

Jinlong Wang[1,2,3,5], Zilong Gu[1,5], Zhe Zhao[4], Yu Mei[1,2,3], Xinyi Ke[1,2,3], Yihao Chen[1,2,3], Gaoshan Huang[1,2,3,*] and Yongfeng Mei[1,2,3,*]

[1] Department of Materials Science & State Key Laboratory of Molecular Engineering of Polymers, Fudan University, Shanghai 200438, People's Republic of China
[2] Yiwu Research Institute of Fudan University, Yiwu 322000, Zhejiang, People's Republic of China
[3] International Institute of Intelligent Nanorobots and Nanosystems, Fudan University, Shanghai 200438, People's Republic of China
[4] College of Biological Science and Medical Engineering, Donghua University, Shanghai 201620, People's Republic of China

E-mail: gshuang@fudan.edu.cn and yfm@fudan.edu.cn

Received 14 April 2024, revised 3 July 2024
Accepted for publication 9 July 2024
Published 19 July 2024

Abstract

Due to shortcomings such as poor homogeneity of Al doping, precisely controlling the thickness, inability to conformally deposit on high aspect ratio devices and high pinhole rate, the applications of Al-doped ZnO (AZO) nanomembrane in integrated optoelectronic devices are remarkably influenced. Here, we report *in situ* monitoring during the atomic layer deposition (ALD) of AZO nanomembrane by using an integrated spectroscopic ellipsometer. AZO nanomembranes with different compositions were deposited with real-time and precise atomic level monitoring of the deposition process. We specifically investigate the half-reaction and thickness evolution during the ALD processes and the influence of the chamber temperature is also disclosed. Structural characterizations demonstrate that the obtained AZO nanomembranes without any post-treatment are uniform, dense and pinhole-free. The transmittances of the nanomembranes in visible range are >94%, and the optimal conductivity can reach up to 1210 S cm^{-1}. The output of current research may pave the way for AZO nanomembrane to become promising in integrated optoelectronic devices.

Supplementary material for this article is available online

Keywords: transparent conductive oxide, AZO nanomembrane, atomic layer deposition, *in situ* monitoring, ellipsometry, transmittance, conductivity

1. Introduction

With the unrelenting growth of the semiconductor industry, transparent conductive films, especially transparent conductive oxides (TCO) films, are presently in high demand across a broad spectrum of fields such as photoelectric displays, solar cells, organic light-emitting diodes, low- emission glass, special functional window coatings and flexible electronic devices [1, 2] owing to their exceptional properties such as high conductivity, excellent visible range transparency, high infrared reflectivity and semiconductor characteristics [3, 4]. TCO primarily encompasses oxides of Sn, In, Cd and Zn, along with their doped counterparts [5]. In_2O_3:Sn (ITO) film is one of the prevalent TCO materials within the industrial realm. Apart from its transparency to visible spectrum and low electrical resistivity, it also exhibits low operating temperature, excellent thermal stability and robust adhesion with

[5] These authors contributed equally to this work.
[*] Authors to whom any correspondence should be addressed.

glass [6, 7], thus making it an ideal candidate for transparent electrode. However, ITO film is detrimental due to its content of toxic indium, posing health risks during its production and application stages. Moreover, natural reserves of key materials such as In and Sn are limited and expensive, and the active chemical nature of Sn and In may poison the substrate during processing [8]. These shortcomings significantly curtail research and application.

Zinc Oxide (ZnO) film, a group II–VI wide bandgap semiconductor material, is non-toxic and affordable, possessing exceptional photoelectric, piezoelectric and dielectric characteristics [9]. Yet, ZnO possesses relatively low conductivity and charge concentration [10]. Introducing Al [11], Cd [12], Ga [13], Mn [14] or In [15] into ZnO film significantly enhances the film's conductivity and overall performance. Previous investigation on Al-doped ZnO (AZO) films demonstrate high transparency across the visible range [16]. They also exhibit extreme chemical stability at high-temperature and in hydrogen plasma environments [17]. Therefore, AZO films are considered promising in optoelectrical devices such as solar cells and liquid crystal displays, among others [18].

AZO film can be grown through sol–gel method [19], magnetron sputtering [20], metal–organic chemical vapor deposition [21], pulsed-laser deposition [22] and atomic layer deposition (ALD) [23]. Among these, sol–gel is a conventional, simple and low-cost method suitable for depositing AZO films on flat substrates with relatively low quality [24]. However, it is challenging to achieve uniform deposition on three-dimensional (3D) structures. Magnetic sputtering can rapidly deposit uniform AZO films on simple 3D substrates [25], but it still faces difficulties in conformal deposition on complex 3D substrates with high aspect ratios (e.g. nanoscale holes and deep trench microdevices). In addition, the thickness control is not precise enough and the densification is not sufficient in these approaches. On the other hand, ALD presents numerous irreplaceable advantages. ALD allows fine-grained control over the ZnO/Al_2O_3 ratio at the atomic scale due to its self-limiting and highly conformal growth [26]. ALD also facilitates conformally depositing evenly dense films on substrates with high aspect ratio structures [27]. These advantages demonstrate good controllability on AZO film. Furthermore, AZO film produced via ALD does not necessitate post-processing operations (such as high-temperature annealing) to attain high electrical conductivity, making it suitable for devices on flexible substrate and with relatively lower processing temperature, i.e. organic transistors [28]. Notably, applications such as photovoltaic devices and liquid crystal displays have stringent demands for the compactness, high conformity and pinhole-free attributes of AZO films [29]. Therefore, investigation on the growth mechanism with the help of *in situ* monitoring of the ALD process to achieve pinhole-free AZO film with high uniformity is of great importance.

Herein, ALD process of AZO nanomembranes was *in situ* monitored by an integrated spectroscopic ellipsometer. The rapid spectral signal fitting ensures real-time and precise measurement of the AZO nanomembrane's thickness and quality. The ALD process parameters are tuned to fabricate AZO nanomembranes with varied layer ratios and growth temperatures, assessing their properties such as conductivity, transmission and band gap. In order to clarify the detailed ALD process, the half-reactions corresponding to production of ZnO and Al_2O_3 are studied extensively. Moreover, the surface composition and structure of each step and the influence of growth temperature on the ALD half-reaction, are analyzed to optimize the ALD process and enhance the nanomembrane quality. The AZO nanomembrane prepared with current ALD approach demonstrates high transmittance and large conductivity without any post-treatment. This work provides experimental evidence for high-quality deposition of AZO films with remarkable potential in optoelectronics.

2. Experimentation

2.1. Material

The single crystal quartz (0001) wafer with dual-side polishing and a surface roughness of $R_a < 1$ nm was procured from Shanghai Prmat Technology Co., Ltd. Diethylzinc (DEZ) and trimethylaluminum (TMA) were acquired from APK (Shanghai) Gas Co., Ltd. Prior to any usage, the wafer underwent multiple cleanings by using acetone, ethanol and deionized water. All deionized (DI) water employed in this experiment was purified through the Millipore system.

2.2. Fabrication of interdigital electrode

The quartz single crystal wafer was diced into rectangles with size of 1×2 cm^2. A uniform photoresist (ARP-3510, Allresist GmbH) layer with a thickness of about 2 μm was spin-coated on the substrate surface. The photoresist layer was then patterned into an interdigital electrode shape by UV lithography (SUSS MA6). A 10 nm Ge/50 nm Au film was then deposited by using magnetron sputtering. The photoresist layer was then cleaned with acetone to enable the preparation of Ge/Au interdigital electrodes for subsequent AZO nanomembrane deposition and electrical characterizations.

2.3. ALD of AZO nanomembrane

Deposition of the AZO nanomembranes was accomplished in our home-made ALD system integrated with *in situ* monitoring module of ellipsometer. ZnO layers were deposited by using DEZ and DI water as precursors. Al_2O_3 layers were deposited by using TMA and DI water as precursors. The carrier gas flowrate is set at 50 sccm. This study was necessitated by carrying out 300 ALD cycle processes at a deposition temperature of 200 °C on both the blank quartz substrate and the substrate with interdigital electrodes. The optimized ALD cycle process encompasses DI water pulse (30 ms), waiting (3 s), N_2 purge (20 s), DEZ or TMA pulse (30 ms), waiting (3 s), and N_2 purge (20 s). AZO nanomembranes with various compositions were prepared by tuning the numbers of cycles corresponding to Al_2O_3 and ZnO. Specifically, the

AZO-9 indicates 54 cycles of ZnO pulses and 6 cycles of Al_2O_3 pulses; AZO-19 it indicates 57 cycles of ZnO pulses and 3 cycles of Al_2O_3 pulses; AZO-29 indicates 58 cycles of ZnO pulses and 2 cycles of Al_2O_3 pulses. All pulse cycle groups are repeated 5 times to ensure the number of total cycles reaches 300. Pure ZnO nanomembrane of 300 ALD cycles was also prepared for comparison. In addition, samples were prepared at different deposition temperatures to investigate the effect of deposition temperature on the properties of AZO nanomembranes.

2.4. In situ monitoring during the ALD process

We integrate a spectroscopic ellipsometer (J.A. Woollam iSE) into our ALD vacuum chamber to realize real-time *in situ* monitoring during the ALD process. Data points during real-time monitoring were collected every 0.1 s with an interval of 2 s. Data analysis was carried out by using Complete EASE software. The Al_2O_3 layer was modelled by using the Cauchy dispersion formula [30], where parameters *a, b* and *c* are assigned to 1.751, 0.006 32 and −0.000 101 52, respectively. For ZnO layer, the Gaussian Oscillator formulae is more appropriate [31], where E_{inf} is set to 1.923, UV Pole Amp is 39.4332, UV Pole En is 7.999 and IR Pole Amp is 0.4196. Two analytical models demonstrate continuous superposition for fitting the AZO nanomembrane depositions by ALD. The switching time of the two analytical models is matched with the ALD deposition of the two materials.

2.5. Structure, optical and electrical characterization of the device

The morphologies of AZO nanomembranes were measured by a field emission scanning electron microscope (ZEISS Sigma 300). The crystallographic structure is detected using an X'Pert ProX-ray diffractometer equipped with Cu Kα radiation ($\lambda = 0.1542$ nm), employing a voltage of 40 keV and current flow of 40 mA. EDS (Oxford Xplore 30) was employed to analyze the compositions and ionic concentrations of these samples. XPS analyses were performed using a Thermo Scientific K-Alpha device. Curve fitting on all XPS spectra is accomplished using XPS Peak 4.1 software. The conductivity of the AZO nanomembrane sample is gauged by means of a four-probe resistivity tester (Helpass HPS2663). The transmittance and band-gap energy of the AZO nanomembrane were evaluated through a UV-visible spectrophotometer (Shimadzu UV-2550), which collected the transmittance and absorbance spectra in the spectral range of 320–800 nm. The electrical characteristics of AZO nanomembrane deposited on interdigital electrodes were explored using a semiconductor analyzer (Keithley SCS-4200).

3. Results and discussion

Figure 1(a) presents the scanning electron microscopy (SEM) images of AZO nanomembranes deposited via ALD with varied Al contents (i.e. 9:1, 19:1, 29:1 and pure ZnO), at a temperature of 200 °C. These AZO nanomembranes, differing from their inhomogeneous, wrinkled and cracked configurations fabricated through sol–gel method as detailed in literature [32], display uniform, dense and voidless morphology. The morphologies of these AZO nanomembranes do not undergo significant alteration with respect to the Al_2O_3 content, proving the layer-by-layer formation of the ALD technology. Figure 1(b) illustrates the XRD spectra of pure ZnO nanomembranes and AZO nanomembranes with varied Al contents. The pure ZnO nanomembrane exhibits a strong diffraction peak corresponding to the (100) plane and a weak diffraction peak to the (002) plane. This illustrates that a large amount of ZnO grows along the (100) plane under ALD growth conditions at 200 °C. Compared with standard JCPDS card, XRD spectra of these nanomembranes indicate that they are multi-crystalline and consistent with the ZnO wurtzite structure [33]. No other diffraction peak from Al-related compound can be detected in the XRD spectra of the AZO nanomembranes. With an increased Al content in the AZO nanomembrane, the intensity of the ZnO (100) diffraction peak decreases. This implies that higher Al content suppresses crystallinity of ZnO, resulting in deterioration of unidirectional structure and multi-directional growth becomes obvious. Moreover, when partial Zn^{2+} ions are replaced by Al^{3+}, a slight shift of the diffraction peak towards higher angle is observed as the radius of the Al^{3+} ions (0.53 Å) is smaller than that of the Zn^{2+} ions (0.74 Å) [34]. The EDX spectrum of AZO-9 nanomembrane is collected to quantitatively analyze the atomic composition, as depicted in figure 1(c). The results affirm that only Zn, O and Al elements exist in the AZO-9 nanomembrane. Additionally, the Zn:O:Al ratio in the AZO-9 nanomembrane conforms to the 9:1 proportion of ZnO and Al_2O_3 layers. This validates ALD's capacity for precise control over the nanomembrane composition on an atomic scale. The chemical composition of the AZO nanomembrane is further verified through XPS analysis. The results confirm the presence of Zn, Al and O (figure S1). Figures 1(d)–(f) respectively show the high-resolution spectra of Zn 2p, Al 2p, and O 1s in AZO-9 nanomembrane. Figure 1(d) demonstrates that positions of Zn $2p^{1/2}$ and Zn $2p^{3/2}$ peaks correspond to those in wurtzite ZnO [35]. Furthermore, the peak at 74.28 eV position of Al 2p in figure 1(e) complies with the bridging Al–O bonding structure [36]. The high-resolution O 1s spectrum can be decomposed into two peaks at 530.28 and 531.98 eV, respectively, corresponding to Zn–O and Al–O bond, as shown in figure 1(f) [37], which are quite different from those prepared by sol–gel method [38].

Figure 2(a) illustrates the ALD chamber and the integrated ellipsometer used for the preparation of AZO nanomembranes. The real-time monitoring and the fitting interfaces are schematically shown. The pulsed introduction of DEZ, H_2O and TMA, as per the ALD deposition sequence, is conducted within an ALD vacuum chamber to achieve growth of AZO nanomembranes with different compositions. The integrated spectroscopic ellipsometer in the ALD chamber enables *in situ* monitoring of the nanomembrane growth during the ALD process, while assessing nanomembrane deposition rate.

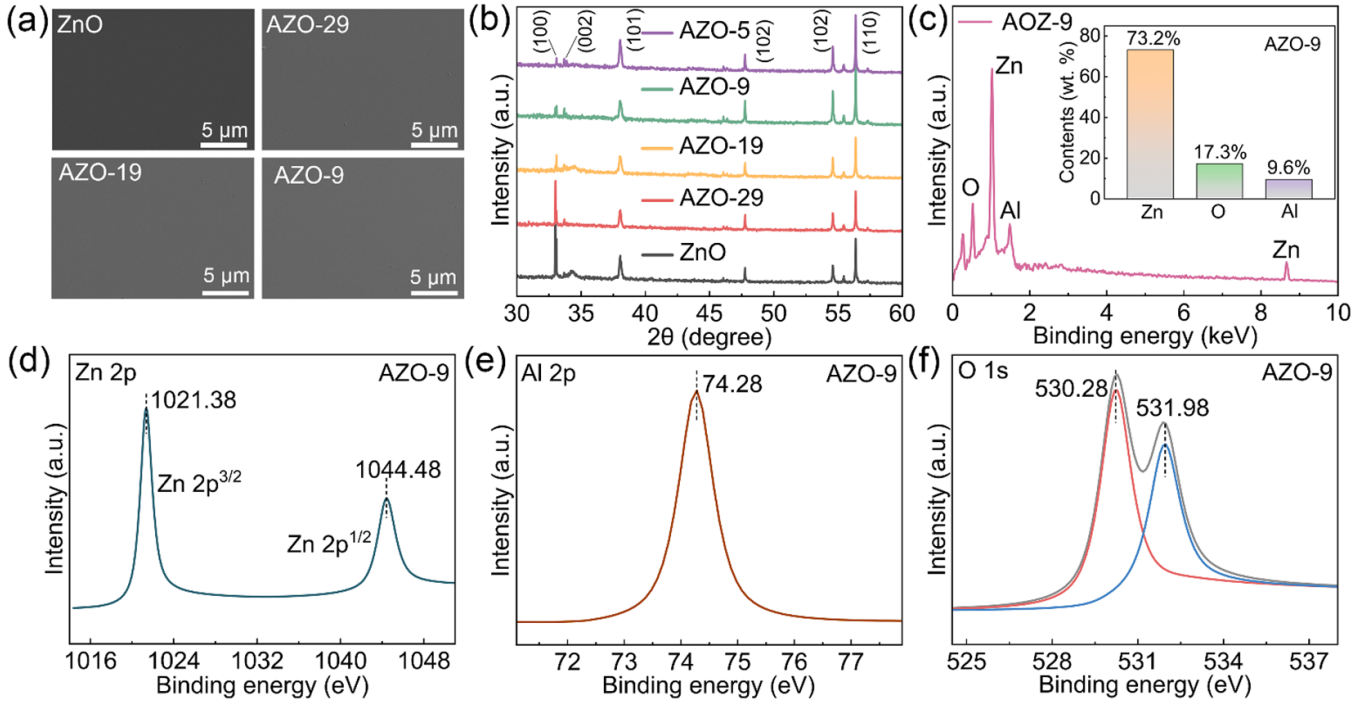

Figure 1. Characterizations of AZO nanomembranes with different ratios deposited by ALD at 200 °C. (a) SEM images of the samples. (b) XRD spectra of the samples. (c) EDX energy spectra of AZO-9 nanomembrane. The inset shows the corresponding atomic concentrations. High-resolution XPS spectra of AZO-9 nanomembrane: (d) Zn 2p, (e) Al 2p and (f) O 1s.

The *Psi* and *Delta* signal data monitored in real time by the ellipsometer during the growth process of AZO-9 nanomembrane are illustrated in figures S2 and S3. Thickness fitting of data obtained via *in situ* ellipsometric spectra is used for the detailed study of the growth of the AZO nanomembrane and the ALD half reaction. Figure 2(b) shows the relation between nanomembrane thickness and deposition time for AZO-9 nanomembrane. As mentioned before, the recipe includes 54 cycles of ZnO layers followed by 6 cycles of Al_2O_3 layers. Thus the thickness-time curves can be fitted by $y = 2.26x + 0.58$ and $y = 1.32x + 45.31$ respectively for ZnO layers and Al_2O_3 layers, while the times used for ZnO and Al_2O_3 cycles are both 46.06 s. Consequently, on the basis of *in situ* monitoring data, at the deposition temperature of 200 °C, ALD deposition rates are 1.73 Å/cycle and 1.10 Å/cycle for ZnO and Al_2O_3 respectively.

Figures 2(c) and (d) showcase the thickness variations of individual cycles (pre-ALD half-reaction and post-ALD half-reaction) of ZnO and Al_2O_3 layers, respectively. For example, in the case of the ZnO layer, during the pre-ALD half-reaction, the chamber is filled with an H_2O pulse, which reacts with the Zn–C_2H_5 bonds on the uppermost surface of the nanomembrane, thereby generating a binder bond of Zn–O–H and emitting CH_4 gas molecules [39]. This process grows a single atomic layer of ZnO. The fitting results of ellipsometric spectra by using a Gaussian Oscillator model indicate an increased thickness of 2.1 Å during this half-reaction. Following N_2 purging, a DEZ pulse is introduced, initiating the post-ALD half-reaction phase. The O–H bond on the uppermost surface of the nanomembrane is broken to produce an O–Zn–CH_3 bond, which also emits CH_4 molecules [39]. This process adds a layer of Zn–CH_3 on surface of nanomembrane, which also causes a change of optical property which can be probed by ellipsometer. Presumably, it would be necessary to construct a Zn–CH_3 model and carry out another fitting task during this dynamic phase. However, due to its short duration, precise real-time switching back and forth between the models for ZnO and Zn–CH_3 cannot be achieved. Therefore, we used the ZnO model with modified optical parameters like refractive index. It is noted that according to the fitting results, the nanomembrane thickness decreases 0.4 Å during the post-ALD half-reaction. However, we believe that this does not indicate that the post-ALD half-reaction caused a reduction in nanomembrane thickness but reflects discrepancies of the fitting model. The average thickness of 1.73 Å for a single ZnO cycle is still accurate and trustable. The ALD cycle will be repeated again after N_2 purging to keep the ZnO nanomembrane growing. For deposition of Al_2O_3, during the pre-ALD half-reaction, the nanomembrane reacts with H_2O to form an Al–O bond [40], which increases the thickness of 2.0 Å. In the post-ALD half-reaction, the nanomembrane reacts with TMA to form O–Al–$(CH_2)_2$ [40], which reduces the thickness of 0.9 Å on the basis of the fitting model. The difference in refractive indexes of the Al–$(CH_2)_2$ and that of the Al_2O_3 layer is relatively larger, leading to a larger discrepancy. As an average effect, one Al_2O_3 cycle corresponds to a thickness of

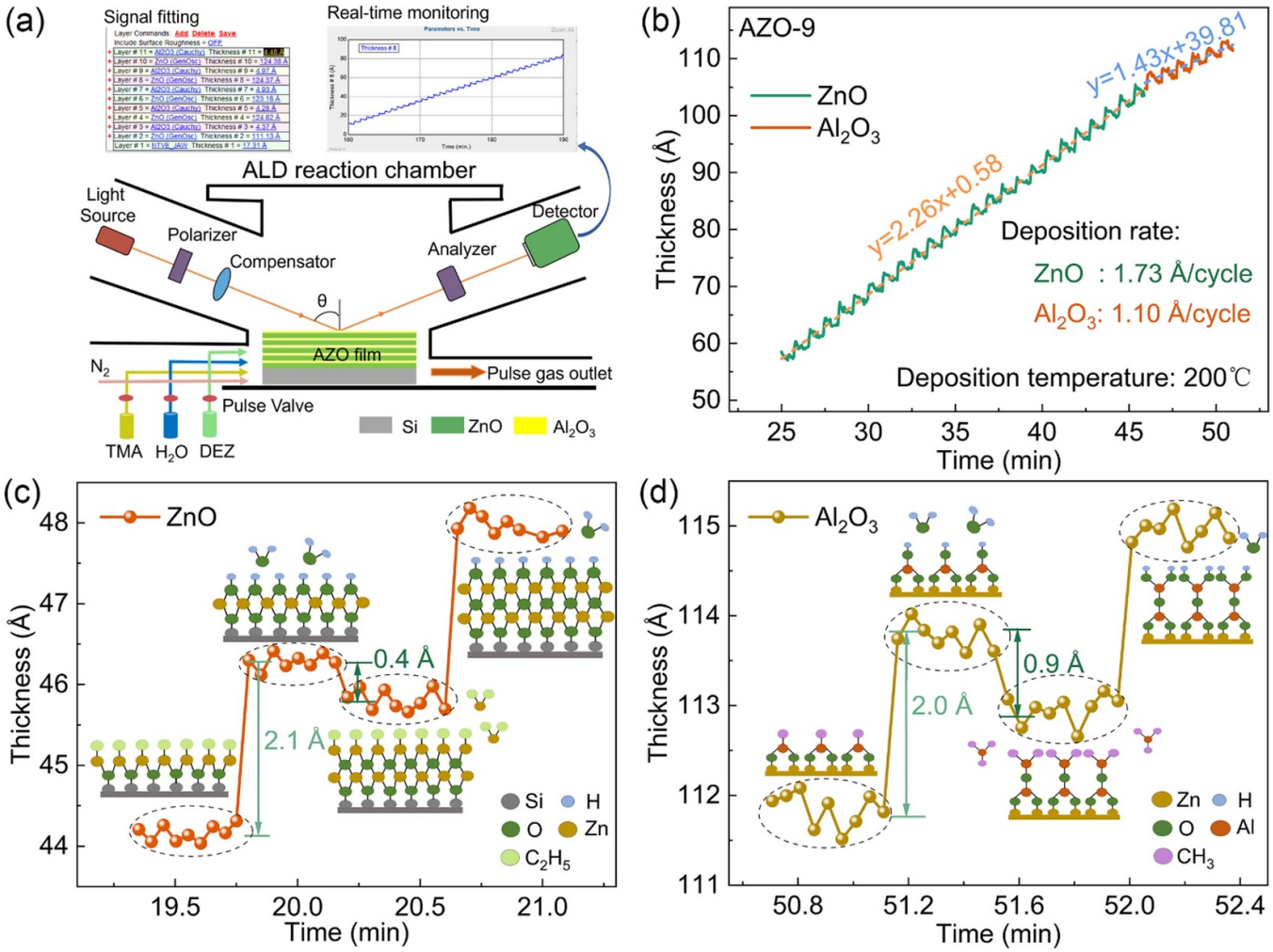

Figure 2. *In situ* monitoring during the ALD of AZO nanomembrane. (a) Schematic of ALD setup with integrated spectroscopic ellipsometer. The real-time monitoring interface and the fitting interface are demonstrated. (b) Relationship between AZO-9 nanomembrane thickness and time, obtained by *in situ* ellipsometry. (c) Thickness variation of individual cycle for ZnO layer and schematic of the growth process at the atomic level. (d) Thickness variations of individual cycle for Al_2O_3 layer and schematic of the growth process at the atomic level.

1.10 Å. Therefore, the ALD-AZO nanomembranes are composed of ZnO/Al_2O_3 layered structure.

The electrical conductivities of the synthesized AZO nanomembranes are measured and the results are illustrated in figure 3(a). The pure ZnO nanomembrane shows extremely low conductivity, while the incorporation of Al_2O_3 layers into ZnO layers leads to a notable increase in conductivity. Moreover, the experimental results demonstrated that the conductivity of AZO nanomembrane is strongly dependent on the Al content. The conductivity reaches a maximum of 1210 S cm^{-1} when the Zn:Al ratio is increased to 9:1 and decreases gradually thereafter. This phenomenon could be ascribed to several effects existing in the AZO nanomembrane, and the situation is relatively complicated. Previously, Lee *et al* [41] found that although layered structure exists in the AZO, Al atoms take oxygen from the ZnO layer and form donors, such as oxygen vacancies or zinc interstitials, thereby enhancing the electrical performance of the nanomembranes. Some research also noticed that Al^{3+} can partially substitute Zn^{2+} to form electron donors at elevated temperature [42]. On the other hand, the substitution should induce lattice strain and create traps that act as recombination centers for electrons [42]. Initially, the carrier concentration rises as Al^{3+} doping quantity escalates, and free electron density in the nanomembrane is mainly determined by the quantity of Al^{3+} dopant. However, as doping quantity reaches a certain threshold, the trap density increases significantly leading to increased carrier recombination. Correspondingly, actual carrier concentration decreases, resulting in diminished conductivity.

In order to ascertain the optical property of AZO nanomembranes with different Al contents, transmission (figure 3(b)) and absorbance spectra (figure S4) for the wavelength range of 320–800 nm were measured. In the visible range, sharp absorption edges due to interband transition can be observed (figure 3(b)). For photon energy below bandgap, the transmittances of all nanomembranes are remarkable (88%–95%), and

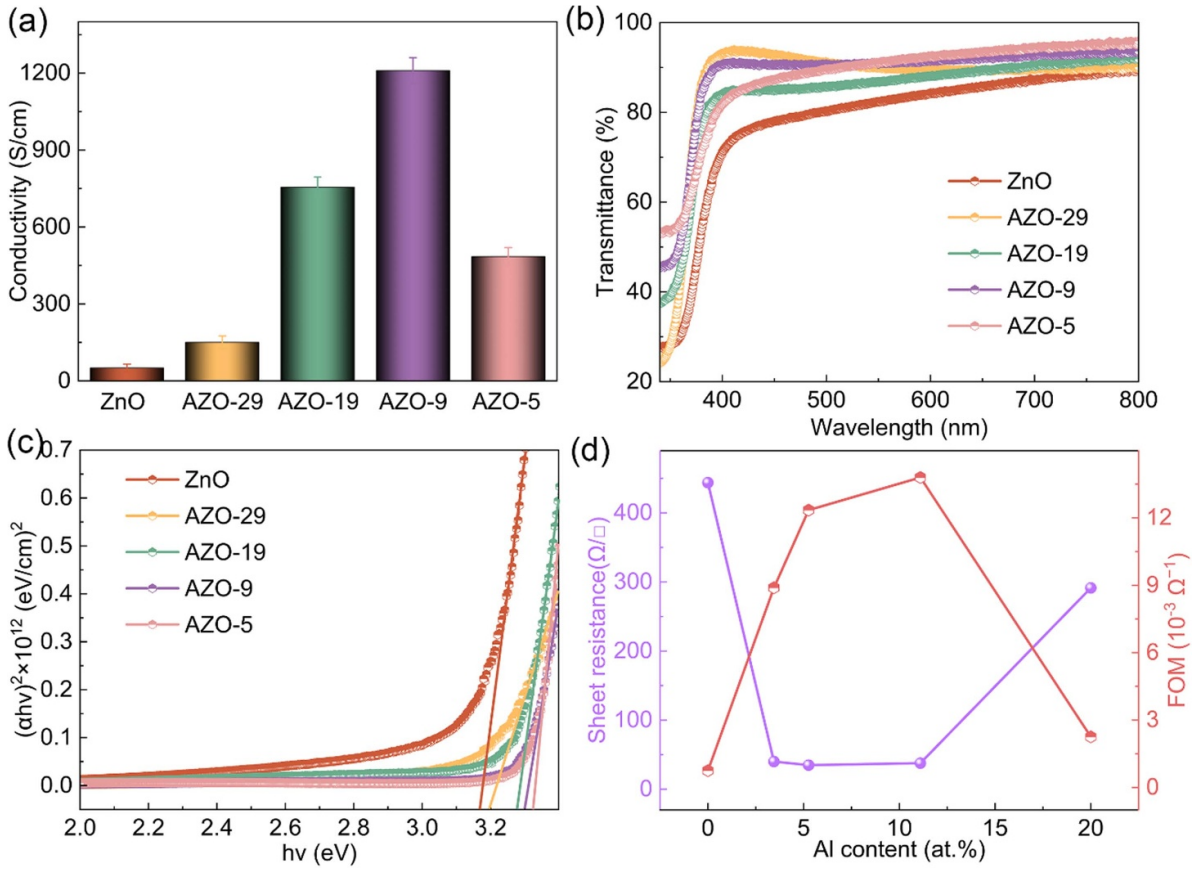

Figure 3. Electrical and optical properties of AZO nanomembranes deposited at 200 °C with different Al contents. (a) Conductivity of the samples. (b) Transmission spectra of samples in the wavelength range of 320–800 nm. (c) $(\alpha h\nu)^2$ vs. $h\nu$ plots (Tauc's graphs) of the samples. (d) Variation of sheet resistance and figure-of-merit of AZO nanomembranes with different Al contents.

the value increases with the Al content. It is worth noting that in previous literature, AZO prepared by other approaches like sol–gel method demonstrates decreased transmittance with increased Al content [32]. This difference may be attributed to the inhomogeneous doping: if Al dopant concentration is substantial in AZO nanomembrane prepared by sol–gel method, clusters of Al could induce considerable random scattering of light [43]. Conversely, AZO nanomembrane deposited layer by layer by using ALD method is obviously uniform, which reduces the scattering of light [44].

Here, the bandgap (E_g) of AZO nanomembrane can be calculated by using following equation [45]:

$$\alpha h\nu = (h\nu - E_g)^{1/2}$$

where $h\nu$ and α signify photon energy and absorption coefficient, respectively, and α is determined by using:

$$ln(1/T) = \alpha d$$

where T and d denote the transmittance and thickness, respectively. The optical bandgap of the film can be obtained by extrapolating the corresponding straight line downwards to the photon energy axis in the Tauc's graph (figure 3(c)). As depicted in figure 3(c), the optical bandgap varies from 3.17 to 3.33 eV with increasing Al content. That is, the cut-off wavelength and absorbance edge of AZO nanomembrane exhibit a 'blueshift' when Al content increases. This could be due to the fact that an increase in carrier concentration due to Al doping would widen the bandgap, leading to a 'blueshift' of the absorbance edge [46].

In addition, to quantitatively evaluate the performance of AZO nanomembranes, a figure-of-merit (FOM) is typically utilized to determine an optimum value for visible light transmittance and sheet resistance, which are the two primary properties of TCO materials. Here, the FOM value (Φ_{TC}) of the obtained AZO nanomembrane can be derived from the following equation [34]:

$$\Phi_T C = T_{ave}^{10}/R_{sh}$$

where T_{ave} is the average transmittance in the wavelength range of 400–800 nm and R_{sh} is the sheet resistance of the nanomembrane. As shown in figure 3(d), the AZO-9 nanomembrane demonstrates a maximum FOM of $13.8 \times 10^{-3}\ \Omega^{-1}$, indicating the current approach of producing AZO with superior optical and electrical properties. We can underscore that the performance of the AZO-9 nanomembrane fabricated with optimized ALD process through *in situ* monitoring can be compared with the properties

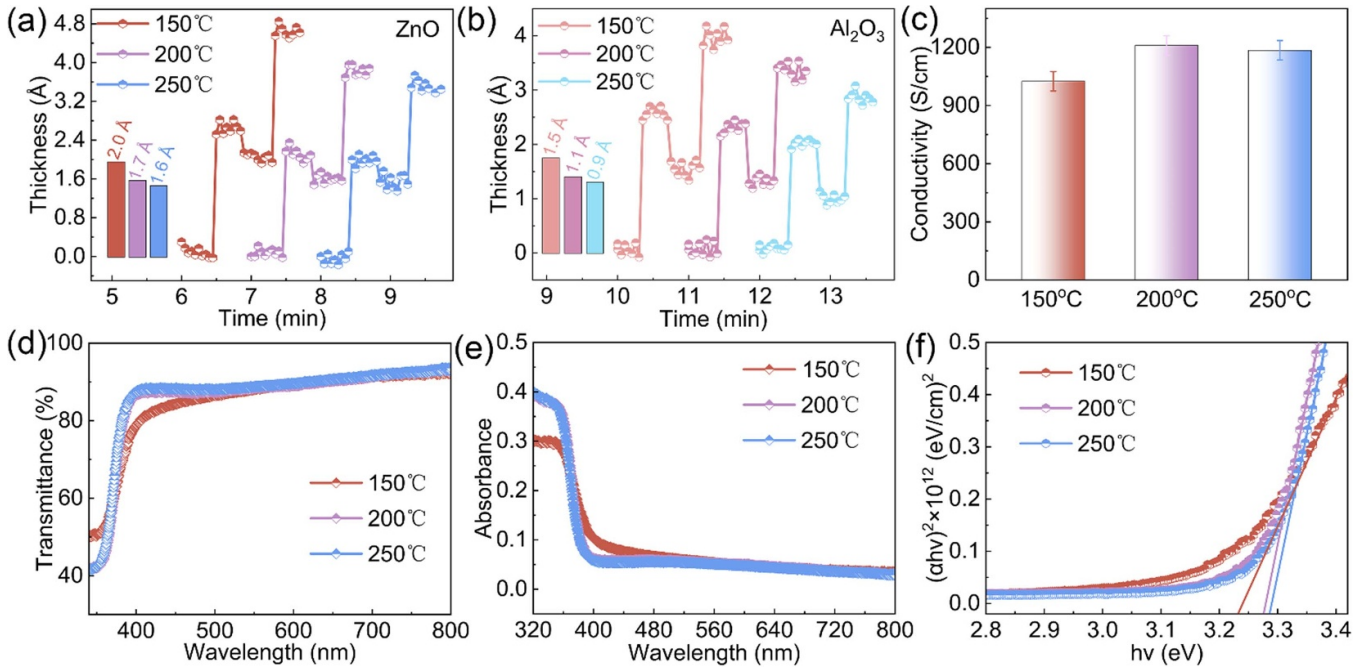

Figure 4. Thickness evolution and physical properties of AZO-9 nanomembranes prepared at different temperatures. (a) and (b) Thickness evolution for ZnO and Al_2O_3 layers deposited by ALD at different temperatures. (c) Conductivity of the samples. (d) Transmission spectra of samples in the wavelength range of 320–800 nm. (e) Absorbance spectra of samples in the wavelength range of 320–800 nm. (f) $(\alpha h\nu)^2$ vs. $h\nu$ plots (Tauc's graphs) of the samples.

of a large number of AZO films prepared by diverse methods as reported previously. A detailed comparison of the optical and electrical properties and FOM values is summarized in table S1.

It is well known that the temperature of the ALD reaction chamber has a significant influence on the deposition process [26]. For this reason, we monitor the real-time growth process of AZO-9 nanomembranes during the ALD at varied temperatures. The thickness evolutions of ZnO and Al_2O_3 layers during the ALD processes are shown in figures 4(a) and (b), respectively. The results show a thickness increase of 2.5 Å in the pre-ALD half-reaction and a decrease of 0.5 Å in the post-ALD half-reaction for ZnO nanomembrane deposited at 150 °C, resulting in an average deposition rate of 2.0 Å/cycle. While the deposition rate decreases to 1.7 and 1.6 Å/cycle at 200 °C and 250 °C, respectively. For Al_2O_3 layers, the deposition rates are 1.5, 1.1 and 0.9 Å/cycle at 150 °C, 200 °C and 250 °C, respectively. The thickness monitoring results of ZnO and Al_2O_3 layers both indicate that as the chamber temperature rises, the deposition rates decrease correspondingly. We consider that when the deposition temperature exceeds the deposition window temperature, part of DEZ/TMA decomposes into atomic Zn/Al and weakly reactive hydrocarbons before contacting the growing surface, and the products connect with –OH to occupy part of the reaction sites [47]. The consumption of the ALD reactive precursors and the occupation of the reaction sites are the reasons for the decreased deposition rate [47]. Conductivity tests are also performed for AZO-9 nanomembranes prepared at different temperatures, as shown in figure 4(c). The conductivity of the AZO-9 nanomembrane deposited at 150 °C is slightly smaller than those at 200 °C and 250 °C. This peculiarity may be due to the lower densities of ZnO and Al_2O_3 produced at 150 °C, and the voids consequently decrease the conductivity [48]. Furthermore, the optical performances of AZO-9 nanomembranes prepared under diverse temperatures (figures 4(d)–(f)) are measured. Except for steep absorption edges, the transmittances of the AZO-9 nanomembranes prepared at three temperatures are all over 94% (figure 4(d)), and the absorbance is below 0.03 (figure 4(e)). According to the relationship between $(\alpha h\nu)^2$ and $h\nu$, the optical bandgaps of the AZO-9 nanomembranes prepared at three temperatures are in the range of 3.23–3.28 V (figure 4(f)). The optical bandgap of the AZO-9 nanomembrane grown at 150 °C is narrower than that of the other two temperatures, which can be attributed to the relatively lower carrier concentration due to the deteriorated nanomembrane quality [45]. Consequently, the ALD chamber temperature for preparing AZO nanomembrane can be adjusted in accordance with the requirements of actual applications to coordinate the tolerable temperature, deposition rate, conductivity, transmittance, and optical bandgap.

4. Conclusion

In conclusion, the spectral ellipsometer integrated within the ALD system accomplishes *in situ* monitoring of growth of AZO during ALD. Specifically, when the layer ratio of ZnO to Al_2O_3 is 9:1, the optimal physical properties, e.g. conductivity of 1210 S cm^{-1}, transmittance of >94%, and bandgap of

3.328 eV, have been achieved without any post-treatment. The half-reaction and thickness variations at each ALD cycle are specifically monitored during the ALD process. At a deposition temperature of 200 °C, the deposition rates are 1.73 Å per cycle and 1.10 Å per cycle for ZnO and Al_2O_3 respectively. The *in situ* monitoring verifies that the deposition temperature influences the deposition rate, conductivity and transmittance of the AZO nanomembranes. The monitoring of growth of nanomembranes helps to understand the growth mechanism at the atomic lever, and optimized AZO nanomembranes with high quality are obtained. The current ALD approach at moderate temperature can be used to prepare AZO and other TCO nanomembranes for various applications especially those devices on fragile substrates.

Data availability statement

All data that support the findings of this study are included within the article (and any supplementary files).

Acknowledgments

This work is supported by the National Key Technologies R&D Program of China (2021YFA0715302), the Science and Technology Commission of Shanghai Municipality (21142200200 and 22ZR1405000), and the National Natural Science Foundation of China (52203328).

ORCID iDs

Jinlong Wang https://orcid.org/0000-0002-1444-0838
Gaoshan Huang https://orcid.org/0000-0002-0525-7177
Yongfeng Mei https://orcid.org/0000-0002-3314-6108

References

[1] Lee D, Song M-S, Seo Y-H, Lee W-W, Kim Y-W, Park M, Shin Y-J, Kwon S-J, Jeon Y and Cho E-S 2024 *Micromachines* **15** 146
[2] Principe J, Duarte V-C-M, Mendes A and Andrade L 2023 *ACS Appl. Energy Mater.* **6** 12442–51
[3] Kumar S and Seo Y 2024 *Small Methods* **8** 2300908
[4] Rozati S-M and Ziabari S-A-M 2022 *Mater. Chem. Phys.* **292** 126789
[5] Zhang D-Y, Yu W-H, Zhang L and Hao X-Y 2023 *Materials* **16** 5537
[6] Ji S-J, Ren H-L, Zhang C-G, Zhao J, Wu H and Dai H-D 2023 *J. Appl. Phys.* **56** 425101
[7] Jenifer K, Arulkumar S, Parthiban S and Kwon J-Y 2020 *J. Electron. Mater.* **49** 7098–111
[8] Hirata A, Fukasawa M, Kugimiya K, Karahashi K, Hamaguchi S and Nagaoka K 2019 *Plasma Process. Polym.* **16** e190002
[9] Telfah A, Al-Bataineh Q-M, Ahmad A-A, Bani-Salameh A-A, Alsaad A-M and Sabirianov R-F 2024 *Appl. Phys.* A **130** 23
[10] Karim A-M-T, Islam M-R, Khatun H, Khan M-K-R, Rahman M-M, Shahjahan M, Hossain M-F, Arif E-M-H and Nazrul-Islam S-M-K 2024 *J. Electron. Mater.* **53** 188–95
[11] de Oliveira G-H-I, Escote M-T, Nantes I-L and Criado D 2024 *J. Am. Ceram. Soc.* **107** 1–9
[12] Lokesha H-S, Prinsloo A-R-E, Mohanty P and Sheppard C-J 2023 *J. Alloys Compd.* **960** 170815
[13] Chen X, Li Y-C, Fei Y, Li D-Y, Wang L, Xie A and Sun D-Y 2024 *Ceram. Int.* **50** 2194–202
[14] Das A, Liu D-Y, Wary R-R, Vasenko A-S, Prezhdo O-V and Nair R-G 2023 *J. Phys. Chem. Lett.* **14** 9604–11
[15] Nuthongkum P, Yansakorn P, Chongsri K, Noonuruk R and Junlabhut P 2023 *J. Mater. Sci., Mater. Electron.* **34** 10
[16] Petrov S *et al* 2023 *Opt. Mater.* **146** 114498
[17] Park H-G, Lee J-H and Yi J 2023 *J. Mater. Sci., Mater. Electron.* **34** 1034
[18] Altuntepe A, Erkan S, Hasret O, Yagmyrov A, Yazici D, Tomakin M, Olgar M-A and Zan R-C 2023 *J. Mater. Sci., Mater. Electron.* **34** 75
[19] Arzaee N-A, Za'abar F-I, Bahrudin M-S, Arsad A-Z, Azman N-I, Abd Rahman M-N, Abdullah W-S-W, Chau C-F and Zuhdi A-W-M 2024 *J. Sol-Gel Sci. Technol.* **110** 52–61
[20] Sarma B, Barman D and Sarma B-K 2019 *Appl. Surf. Sci.* **479** 786–95
[21] Ayinde S-A, Fasakin O, Olofinjana B, Adedeji A-V, Oyedare P-O, Eleruja M-A and Ajayi E-O-B 2019 *J. Electron. Mater.* **48** 3655–61
[22] Park S, Ikegami T and Ebihara K 2005 *Jpn. J. Appl. Phys.* **44** 8027–31
[23] Kan Z-P, Wang Z-W, Firdaus Y, Babics M, Alshareef H-N and Beaujuge P-M 2018 *J. Mater. Chem.* A **6** 10176–83
[24] Singh M and Scotognella F 2023 *Micromachines* **14** 536
[25] Zhao Y-F, Ding W, Xiao Y-B and Yang P 2023 *Vacuum* **210** 111849
[26] Li J-X, Chai G-D and Wang X-W 2023 *Int. J. Extrem. Manuf.* **5** 032003
[27] Tung N-T, Saito S, Sasaki T, Greif D, Parsons M-F, Holmes S and Hane K 2023 *J. Microelectromech. Syst.* **32** 352–61
[28] Luka G, Godlewski M, Guziewicz E, Stakhira P, Cherpak V and Volynyuk D 2012 *Semicond. Sci. Technol.* **27** 074006
[29] Chen R, Cao K, Wen Y-W, Yang F, Wang J, Liu X and Shan B 2024 *Int. J. Extrem. Manuf.* **6** 022003
[30] Smith D-Y, Inokutil M and Karstens W 2001 *J. Phys.: Condens. Matter* **13** 3883
[31] Jellison G-E and Modine F-A 1996 *Appl. Phys. Lett.* **69** 371
[32] Raj R, Gupta H and Purohit L-P 2021 *Pramana J. Phys.* **95** 87
[33] Yu Q, Zhao H-W and Zhao Y 2024 *Curr. Appl. Phys.* **57** 111–8
[34] Bui Q-C *et al* 2023 *Materialia* **31** 101863
[35] Lee H-J, Kim J-H, Park S-S, Hong S-S and Lee G-D 2015 *J. Ind. Eng. Chem.* **25** 199–206
[36] Chaukulkar R-P, Thissen N-F-W, Rai V-R and Agarwal S 2014 *J. Vac. Sci. Technol.* A **32** 01A108
[37] Labis J-P, Albrithen H-A, Hezam M, Shar M-A, Algarni A, Alhazaa A-N, El-Toni A-M and Alduraibi M-A 2023 *Nanomaterials* **13** 1345
[38] Nimbalkar A-R, Patil N-B, Ganbavle V-V, Mohite S-V, Madhale K-V and Patil M-G 2019 *J. Alloys Compd.* **775** 466–73
[39] Ott A-W, Klaus J-W, Johnson J-M, George S-M, McCarley K-C and Way J-D 1997 *Chem. Mater.* **9** 707–14

[40] Li Y, Yao R, Wang H-H, Wu X-M, Wu J-Z, Wu X-H and Qin W 2017 *ACS Appl. Mater. Interfaces* **9** 11711–20
[41] Lee D-J, Kim H-M, Kwon J-Y, Choi H, Kim S-H and Kim K-B 2011 *Adv. Funct. Mater.* **21** 448–55
[42] Bandaru N and Panda E 2019 *Mater. Sci. Semicond. Process.* **100** 220–4
[43] Ghasedi A, Koushki E, Zirak M and Alehdaghi H 2020 *Appl. Phys.* A **126** 474
[44] Koskinen T, Raju R, Tittonen I and Kauppinen C 2023 *Appl. Phys. Lett.* **123** 011902
[45] Rajput J-K, Pathak T-K, Kumar V, Kumar M and Purohit L-P 2017 *Surf. Interfaces* **6** 11
[46] Upadhyay G-K, Rajput J-K, Pathak T-K, Kumar V and Purohit L-P 2019 *Vacuum* **160** 154
[47] Xia B, Ganem J-J, Briand E, Steydli S, Tancrez H and Vickridge I 2021 *Vacuum* **190** 110289
[48] Badie C *et al* 2023 *J. Vac. Sci. Technol.* A **41** 03240